Nonviral Nanoscale-Based Delivery of Antisense Oligonucleotides Targeted to Hypoxia-Inducible Factor 1α Enhances the Efficacy of Chemotherapy in Drug-Resistant Tumor

Yang Wang,[1] Maha Saad,[1] Refika I. Pakunlu,[1] Jayant J. Khandare,[1] Olga B. Garbuzenko,[1] Alexandre A. Vetcher,[2] Viatcheslav A. Soldatenkov,[3] Vitaly P. Pozharov,[1] and Tamara Minko[1,4]

Abstract

Purpose: To enhance the efficacy of cancer treatment, we propose a complex approach: simultaneous delivery to the tumor of a chemotherapeutic agent and a suppressor of hypoxia-inducible factor 1α (HIF1A).

Experimental Design: The novel complex liposomal drug delivery system was developed and evaluated *in vitro* and *in vivo* on nude mice bearing xenografts of multidrug-resistant human ovarian carcinoma. The proposed novel complex drug delivery system consists of liposomes as a nanocarrier, a traditional anticancer drug (doxorubicin) as a cell death inducer, and antisense oligonucleotides targeted to HIF1A mRNA as a suppressor of cellular resistance and angiogenesis.

Results: The system effectively delivers active ingredients into tumor cells, multiplies the cell death signal initiated by doxorubicin, and inhibits cellular defensive mechanisms and angiogenesis by down-regulating BCL2, HSP90, and vascular endothelial growth factor proteins. This, in turn, activates caspases, promotes apoptosis, necrosis, and tumor shrinkage. The proposed novel complex multipronged approach enhances the efficiency of chemotherapy.

Conclusions: The proposed combination therapy prevents the development of resistance in cancer cells, and thus, increases the efficacy of chemotherapy to an extent that cannot be achieved by individual components applied separately. It could form the foundation for a novel type of cancer therapy based on simultaneous delivery of an anticancer drug and a suppressor of HIF1A.

The efficacy of cancer chemotherapy is mainly limited by the rapid development of tumor multidrug resistance (1–3). One of the important mechanisms of cancer resistance to chemotherapy is the adaptation of cancer cells to tumor hypoxia (4–7). Hypoxia occurs in solid tumors starting from the early stages of tumor development (7) as a result of an inadequate supply of oxygen, due to exponential cellular proliferation and an insufficient blood supply (6). The resulting glucose deprivation and oxygen deficit play a bimodal role in tumor development and survival (8, 9). On the one hand, these conditions induce cell death by apoptosis and necrosis (7, 10–13). On the other hand, they initiate adaptation to hypoxia and increase tumor resistance to anticancer drugs (5, 14, 15). Hypoxia therefore presents a paradox by imposing negative effects on cell growth and simultaneously inducing mitigating responses that oppose the negative effects by driving critical tumorigenic adaptations (4, 10, 12, 16). In most cases, hypoxia is an adverse prognostic indicator in cancer because it is associated with tumor progression and resistance to therapy (6, 7, 9).

Hypoxia-inducible factor-1 (HIF1A) plays an essential role in cellular, and ultimately, systemic homeostatic responses to hypoxia (11, 17, 18). Previously, we have shown that HIF1A induces a bimodal cellular response to hypoxia (8). In the first mode, the activation of this protein by hypoxia triggers apoptotic and necrotic cell death pathways. In the counter mode, hypoxia through the activation of the HIF1A transcriptional factor increases cellular antiapoptotic defense, and improves the mitochondrial respiration and stability of its membranes by the overexpression of the BCL2 protein. These processes substantially limit apoptotic cell death induced by hypoxia. It was found that in cancer cells, the balance between these two processes—the damaging and protective effects of hypoxia—slightly favor the induction of cell death (8). We hypothesize that in order to facilitate the cytolethal potential of endogenous tumor hypoxia by preventing the development of antiapoptotic defensive mechanisms in cancer cells, this balance should be further shifted towards cell death by the inhibition of the overexpression of HIF1A.

Authors' Affiliations: [1]Department of Pharmaceutics, Rutgers, The State University of New Jersey, Piscataway, New Jersey; [2]National Center for Biodefense and Infectious Diseases, George Mason University, Manassas, Virginia; [3]Department of Radiation Medicine, Lombardi Comprehensive Cancer Center, Georgetown University Medical Center, Washington, District of Columbia; and [4]Cancer Institute of New Jersey, New Brunswick, New Jersey

Received 8/15/07; revised 12/9/07; accepted 2/6/08.

Grant support: NIH grants CA100098, CA111766, and CA074175 from the National Cancer Institute.

The costs of publication of this article were defrayed in part by the payment of page charges. This article must therefore be hereby marked *advertisement* in accordance with 18 U.S.C. Section 1734 solely to indicate this fact.

Requests for reprints: Tamara Minko, Department of Pharmaceutics, Ernest Mario School of Pharmacy, Rutgers, The State University of New Jersey, 160 Frelinghuysen Road, Piscataway, NJ 08854-8020. Phone: 732-445-3831, ext. 214; Fax: 732-445-3134; E-mail: minko@rci.rutgers.edu.

©2008 American Association for Cancer Research.

doi:10.1158/1078-0432.CCR-07-2020

Downloaded from clincancerres.aacrjournals.org on September 21, 2019. © 2008 American Association for Cancer Research.

We are proposing a novel nonviral nanoscale-based hypoxia-inducible factor–targeted anticancer drug delivery system which includes three main components (*a*) coated with poly(ethylene glycol) polymer (PEGylated) liposomes as drug carriers, (*b*) doxorubicin as a cell death–inducing agent (anticancer drug), and (*c*) antisense oligonucleotides (ASO) targeted to HIF1A mRNA as a suppressor of cellular signaling pathways triggered by hypoxia-inducible transcriptional factor, and ultimately, cellular resistance to chemotherapy. This system is expected to provide for an efficient systemic delivery to the tumor and uptake by cancer cells of an anticancer drug and ASO targeted to HIF1A mRNA in order to simultaneously induce cell death and suppress HIF1A protein and therefore enhance the efficacy of chemotherapy.

Materials and Methods

Drug, ASOs, and liposomal delivery system. The complex liposomal drug delivery system included the following components: (*a*) a carrier—conventional or PEGylated liposomes, (*b*) an apoptosis inducer—a traditional anticancer drug doxorubicin, and (*c*) ASO targeted to HIF1A mRNA. Doxorubicin was obtained from Sigma. The sequence of the ASOs targeted to HIF1A mRNA was 5′-GCC GGC GCC CTC CAT-3′ (8, 19). The DNA backbone of all bases in oligonucleotides was P-ethoxy–modified to enhance nuclease resistance and increase incorporation efficacy into liposomes. ASO were synthesized by Oligos, Etc. ASO and doxorubicin (Sigma) were packaged in liposomes, which were prepared using the previously described lipid film rehydration method (20). To prepare conventional liposomes, lipids (Avanti Polar Lipids) were dissolved in chloroform, evaporated to a thin film in a rotary evaporator, and rehydrated with citrate buffer. The lipid ratio for all formulations was 7:3:10 (v/v, egg phosphatidylcholine/1,2-dipalmitoyl-*sn*-glycero-3-phosphatidylcholine/cholesterol). To prepare PEGylated liposomes, egg phosphatidyl choline, cholesterol, and DSPE-PEG (1,2-distearoyl-*sn*-glycero-3-phosphoetanol amine-*N*-aminopolyethylene glycol—M_w ~2,000 ammonium salt) were dissolved in 4.0 mL of chloroform with 1.85:1:0.15 molar ratio, respectively (all compounds were obtained from Avanti Polar Lipids). The clear lipid solution was evaporated at 25°C under reduced pressure. The thin layer was formed and rehydrated using 2.0 mL of 0.3 mol/L sodium citrate buffer (pH 4.0). The lipid mixture was sonicated continuously for 3.0 h to obtain stealth liposomes. The liposomes were freeze-thawed under liquid nitrogen and placed in -20°C overnight. ASO were loaded into the liposomes by dissolving ASO in the rehydration buffer at a concentration of 0.5 mmol/L. Doxorubicin was loaded passively by dissolving in the rehydration buffer with the ASO (0.16 w/w doxorubicin/lipid ratio). After preparation, free doxorubicin and ASO were separated from conventional liposomes by passing the liposome suspension through a Sephadex G50 column. PEGylated liposomes with encapsulated doxorubicin were separated from free drug by dialysis, whereas unbound doxorubicin and ASO were separated from loaded PEGylated liposomes by filtration at 4,000 × *g* within 20 min through Amicon Ultra-15 Centrifugal Filter (10,000 WCO; Millipore Corporation). The encapsulation efficacy ranged from 51.5% to 58.3% in different series of experiments. The diameter and shape of liposomes were measured by dynamic light scattering and an atomic force microscope. The liposome diameter ranged from 100 to 200 nm. A series of *in vitro* experiments established the stability of the liposomes containing fluorescent ASO and doxorubicin. Liposomes incubated in saline for several weeks did not release any significant amount of labeled ASO.

Cell line. The human multidrug-resistant ovarian carcinoma A2780/AD cell line was obtained from Dr. T.C. Hamilton (Fox Chase Cancer Center, Philadelphia, PA). Cells were cultured in RPMI 1640 medium (Sigma) supplemented with 10% fetal bovine serum (Fisher Chemicals). Cells were grown at 37°C in a humidified atmosphere of 5% CO_2 (v/v) in air. All experiments were done on cells in the exponential growth phase.

Animal tumor model and antitumor activity. An animal model of human ovarian carcinoma xenografts was used as previously described (21–24). Briefly, A2780/AD human multidrug-resistant ovarian cancer cells (2×10^6) were subcutaneously transplanted into the flanks of female athymic *nu/nu* mice. When the tumors reached a size of ~0.3 cm^3 (15-20 days after transplantation), mice were treated i.p. with (*a*) saline (control), (*b*) free ASO targeted to HIF1A mRNA, (*c*) empty PEGylated liposomes, (*d*) liposomal ASO targeted to HIF1A mRNA, (*e*) free doxorubicin, (*f*) free doxorubicin mixed with liposomal ASO targeted to HIF1A mRNA, (*g*) liposomes containing doxorubicin, (*h*) liposomes containing doxorubicin mixed with free ASO targeted to HIF1A mRNA, (*i*) a mixture of liposomal doxorubicin with liposomal ASO targeted to HIF1A mRNA, and (*j*) liposomes containing both doxorubicin and ASO targeted to HIF1A mRNA in one vesicle. The dose of all formulations containing doxorubicin (2.5 mg doxorubicin/kg in 0.1 mL for the single injection) corresponds to the maximum tolerated dose of free doxorubicin. The maximum tolerated dose of doxorubicin was estimated in separate experiments based on animal weight change after the injection of increasing doses of doxorubicin as previously described (21–24). Animal weight was measured every day within 1 week after the treatment. Changes in tumor size were used as an overall marker for antitumor activity as previously described (21–24).

In vivo *imaging*. PEGylated liposomes were labeled with near-IR fluorophore cyanine dye (Cy 5.5). Labeling was done by adding Cy 5.5 (M_w ~1,128; GE Healthcare Bio-Sciences Corp.) and lipid egg phosphatidyl choline, cholesterol, and DSPE-PEG (M_w ~2,000 ammonium salt) in 4.0 mL of chloroform at a molar ratio of 1.85:1:0.15, respectively (all compounds obtained from Avanti Polar Lipids). The content was evaporated to a thin film under pressure using a rotary evaporator. The thin film formed was rehydrated with citrate buffer (pH 5.0). The Cy 5.5 with lipid mixture was sonicated extensively for 4.0 h to obtain the stealth liposomes. The liposomes were freeze-thawed under liquid nitrogen and placed in -20°C overnight. Liposomes were resuspended at room temperature to remove untrapped Cy 5.5 using dialysis membrane (molecular weight cutoff ~2,000 Da) in citrate buffer as a solvent. The conjugate was further purified by size exclusion G10 Sephadex column chromatography. *In vivo* body distribution of labeled liposomes was studied by the IVIS Imaging System (Xenogen) in anesthetized animals according to the instructions of the manufacturer. Animals were anesthetized with isoflurane using the XGI-8 Gas Anesthesia System (Xenogen). Visible light and fluorescent images were taken and overlaid using the manufacturer's software to obtain a composite image. The distribution of fluorescence was analyzed using an original software program developed in our laboratory.

Atomic force microscopy. Atomic force microscopy imaging of conventional and PEGylated liposomes was conducted in tapping mode which is generally described elsewhere (25). Briefly, 50 μL of the liposome suspension in water was applied on freshly cleaved mica, and kept for 10 min at 100% humidity to achieve particle deposition. After removal of the excess water by the gentle touch of the side of mica with the piece of filter paper, liposomes were dried under the gentle flow of dry nitrogen. The images were acquired in dry air with a Nano-R atomic force microscopy instrument (Pacific Nanotechnology, Inc.) in close contact mode using tapping mode etched OMCL-AC160TS silicon probes (Olympus Optical, Co.; ref. 26). The images were processed, and the measurements were done with Femtoscan software v. 2.2.85(5.1) (Advanced Technologies Center). For statistics, no less than 50 unobstructed PEG polymer conjugates were analyzed.

Intracellular localization of liposomes and release of doxorubicin and ASOs. To analyze intracellular localization of ASO released from liposomes, a portion of oligonucleotides were labeled by FITC prior to incorporation into the liposomes. The labeling was done by Oligos, Etc.

Downloaded from clincancerres.aacrjournals.org on September 21, 2019. © 2008 American Association for Cancer Research.

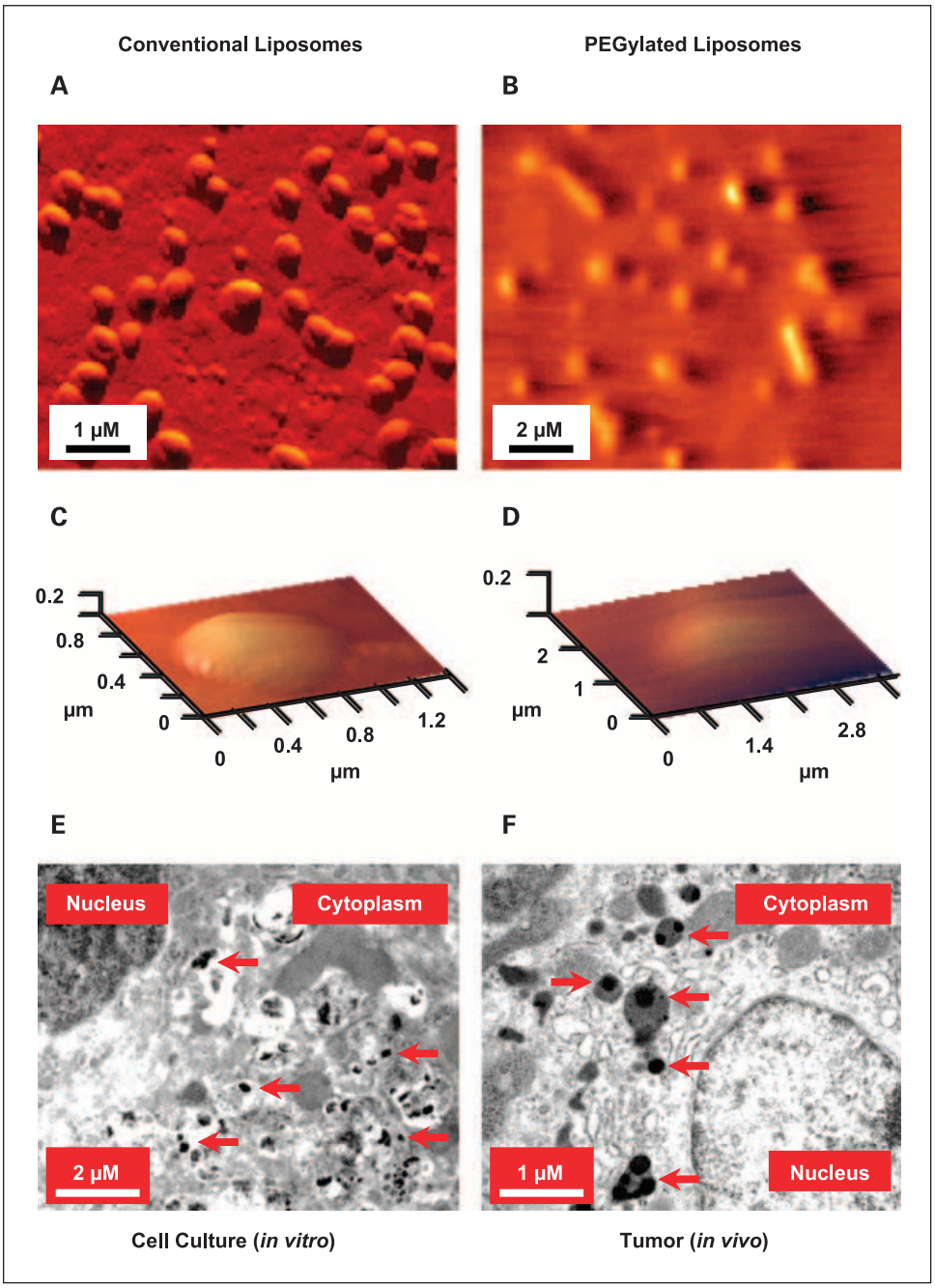

Fig. 1. Assessment of conventional and PEGylated liposomes by atomic force and electron microscopy. *A* to *D,* typical atomic force microscope images of conventional (*A* and *C*) and PEGylated (*B* and *D*) liposomes. Liposome suspensions were applied on freshly cleaved mica, kept for 10 min at 100% humidity atmosphere to achieve deposition and dried under nitrogen flow to remove external water. Panoramic view of conventional (*A*) and PEGylated (*B*) liposomes captured in dem mode (phase contrast). *C* and *D,* three-dimensional zoomed images in height mode (topography). *E* and *F,* transmission electron microscopy images of multidrug-resistant A2780/AD human ovarian carcinoma cells (*E*) and tumor tissue section obtained from mouse bearing xenograft of multidrug-resistant A2780/AD human ovarian carcinoma (*F*) treated with conventional and PEGylated liposomes, respectively. Liposomes were labeled with osmium tetroxide. Arrows, liposomes. The samples for analysis were taken at the end of the experiments (day 6 after the treatment).

These labeled ASO were used only in ASO release and localization experiments. Intracellular localization of ASO and doxorubicin (which possesses intrinsic fluorescence) was studied by fluorescent and confocal microscopy. The release of doxorubicin from liposomes was examined by confocal microscopy in living cells at 37°C within 1 h. Because the fluorescence of doxorubicin and labeled ASO inside liposomes was suppressed, red fluorescence registered inside cancer cells reflects the concentration of released components from the liposomal delivery system.

Labeling of liposomes for electron transmission microscopy was done by adding osmium tetroxide (0.5%) to the rehydration buffer. Cells and tissue sections were fixed prior to electron microscopy using standard techniques as previously described (24, 27). Briefly, cells and tumor tissue were fixed for 2 h in Trump's EM Fixative [combination of a low concentration of both formaldehyde and glutaraldehyde in 0.1 mol/L of Milloning's phosphate buffer (pH 7.3)]. Postfixation was carried out in 1% osmium tetroxide in buffer for 1 h followed by dehydration in graded ethanol series and embedded in Spurr's low-viscosity resin. Sections were prepared using a diamond knife by LKB-2088 Ultramicrotome (LKB-Produkter). Observation and micrographs were made with a JEM-100CXII Electron Microscope (JEOL, Ltd.). Intracellular localization of liposomes was studied in cell culture experiments and in tumor slices.

Gene and protein expression. Quantitative reverse transcriptase-PCR (RT-PCR) was used for the analysis in tumor tissue homogenates of expression of genes encoding HIF1A, P53, HSP90, BAX, BCL2 protein, caspase 3 (*CASP3*) as previously described (8, 19, 20). RNA was isolated using an RNeasy kit (Qiagen). Gene expression was calculated as the ratio of mean band density of analyzed RT-PCR product to that of the internal standard (β_2-microglobulin).

Downloaded from clincancerres.aacrjournals.org on September 21, 2019. © 2008 American Association for Cancer Research.

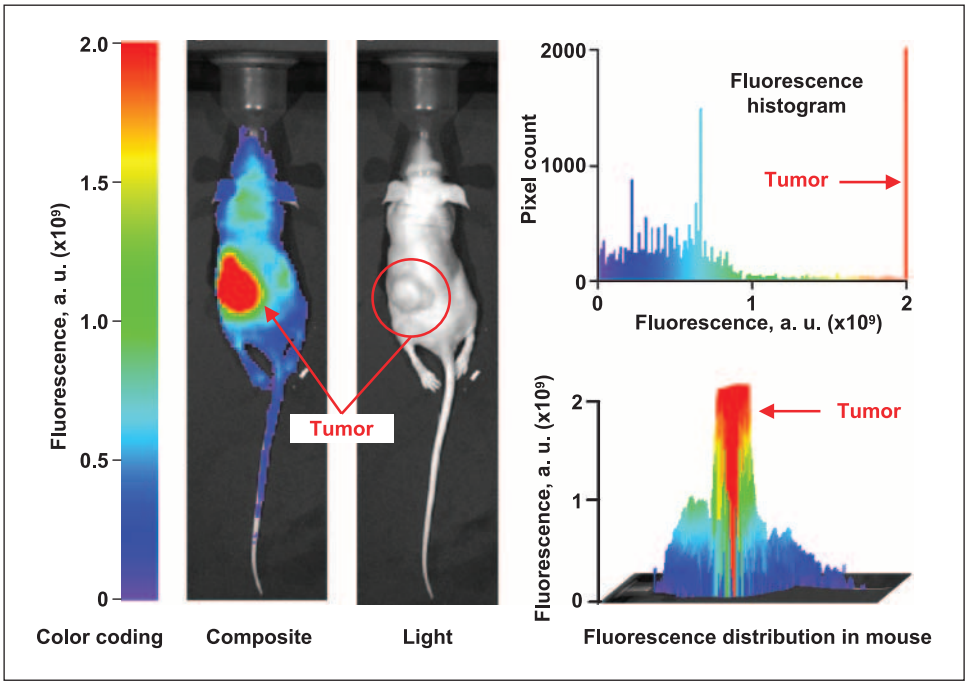

Fig. 2. Body distribution of PEGylated liposomes. Typical *in vivo* images of mouse bearing xenograft of multidrug-resistant A2780/AD human ovarian carcinoma. The mouse was injected with PEGylated liposomes labeled with near-IR fluorophore cyanine dye (Cy 5.5). Images were taken using the IVIS Imaging System (Xenogen) in anesthetized animals at the end of the experiments (day 6 after the treatment). Visible light and fluorescent images were overlaid to obtain a composite image. The distribution of fluorescence was analyzed using an original software program developed in our laboratory.

To confirm RT-PCR data, the expression of HIF1A protein and caspase 9 was analyzed. The identification of HIF1A protein was made by immunohistochemical staining of paraffin-embedded tumor tissue sections. After deparaffinization and rehydration, the slides were stained using the Vector mouse-on-mouse immunodetection kit (Vector Laboratories, Inc.). Mouse monoclonal antibody to HIF1A (1:100 dilution) obtained from StressGen Bioreagents were used as the primary antibody. Biotinylated anti-mouse IgG reagent (1:250 dilution; Vector Laboratories, Inc.) and HSP-Streptavidine detection system (1:500 dilution; Vector Laboratories) in combination with 3,3′-diaminobenzidine substrate kit for peroxidase were used for visualization. After staining, the slides were analyzed by light microscopy and photographed.

The identification of caspase 9 was made by Western immunoblotting analysis and processed using scanning densitometry to quantify the expressed protein. To this end, harvested cells were lysed in radioimmunoprecipitation assay buffer (Santa Cruz Biotechnologies, Inc.) using a needle and syringe. Following incubation on ice for 45 min, the cells were centrifuged at 10,000 × *g* for 10 min. Protein content in the supernatant was determined using the BCA Protein Assay Kit (Pierce) and 50 μg of protein was run on a 15% SDS-polyacrylamide gel immersed in Tris/glycine/SDS buffer (Bio-Rad) for 90 min at 70 V. Protein was transferred to an Immobilon-P nitrocellulose membrane (Millipore) in a Tris/glycine buffer (Bio-Rad) for 90 min at 100 V. The membrane was blocked in nonfat milk for 30 min at room temperature on a rotating shaker to prevent nonspecific binding, washed and incubated overnight with anti–caspase 9 rabbit primary antibody (1:500 dilution; StressGen Biotechnologies) or anti–β-actin mice primary antibody (1:2,000 dilution; Oncogene Research) at 4°C. After washing, the membrane was immersed in goat anti-rabbit and goat anti-mouse IgG biotinylated antibody (1:3,000 dilution and 1:1,000 dilution, respectively; Bio-Rad) at room temperature for 1.5 h on a rotating shaker. Bands were visualized using an alkaline phosphatase color development reagent (Bio-Rad). The bands were digitally photographed and scanned using the Gel Documentation System 920 (NucleoTech). β-Actin was used as an internal standard to normalize protein expression. Protein expression was calculated as the percentage of the β-actin band intensity, which was set at 100%.

Cell death. Two approaches were used to assess apoptosis induction. The first approach was based on the measurement of the enrichment of histone-associated DNA fragments (mononucleosomes and oligonucleosomes) in homogenates of the tumor, liver, and heart using anti-histone and anti-DNA antibodies by a cell death detection ELISA Plus kit (Roche) as previously described (20–22, 24). The second approach was based on the detection of single- and double-stranded DNA breaks (nicks) by an *in situ* cell death detection kit (Roche) using terminal deoxynucleotidyl transferase mediated dUTP-fluorescein nick-end labeling method as previously described (8, 19). Histologic examination of tumor sections was done after H&E staining of samples.

Statistical analysis. Data obtained were analyzed using descriptive statistics, single-factor ANOVA, and presented as mean value ± SD from four to eight independent measurements in separate experiments.

Results

Liposome structure and size. To characterize the structure and size of conventional and PEGylated liposomes, we used atomic force microscopy, a technology with the capability of imaging of wide variety of nanoscale and microscale objects, including liposomes under physiologic conditions. Atomic force microscopy is preferred for the identification of soft surface water–containing nanoparticles versus conventional electron microscopy which has specific requirements for sample preparation such as complete removal of water from the samples and special procedures of staining to increase the contrast of image. The atomic force microscopy images of the liposome preparations (Fig. 1A-D) revealed the convex meniscus shape of the lipidic vesicles. To assess the effects of PEG modification on the structure of liposome vehicles, the images were captured in two modes: "height" which shows the topography of the surface and "dem", which works as a phase contrast and is particularly suitable for object edge detection. As expected, PEGylation of the liposome surface leads to hiding of the object topology (Fig. 1C and D), although individual particles maintain their convex profile. Importantly, each particle has a structure of convex meniscus reflecting the flattening of liposomes during deposition. This

Downloaded from clincancerres.aacrjournals.org on September 21, 2019. © 2008 American Association for Cancer Research.

effect of liposome flattening on the surface of the mica apparently results in the distortion of their actual shape and sizes in water suspension.

PEGylated liposomes accumulated predominantly in the tumor, penetrated into tumor cells providing cytoplasmic and nuclear delivery of doxorubicin and ASO. To estimate the ability of PEGylated liposomes to deliver their payload specifically to tumors and examine the penetration of liposomes inside tumor cells, a series of three experiments were carried out. In the first series, PEGylated liposomes were labeled with Cy 5.5 near-IR dye and their distribution in the body of mice bearing xenografts of A2780/AD multidrug-resistant human ovarian carcinoma were analyzed using the IVIS Imaging System (Xenogen). We found that PEGylated liposomes accumulated predominantly in the tumor (Fig. 2). To further investigate the location of liposomes in the tumor, in the second series of the experiments, we labeled the lipid membrane of the liposomes with osmium tetroxide and analyzed fixed tumor slices by the use of transmission electron microscopy. The liposomes were visualized inside the tumor cell cytoplasm preferentially inside cellular organelles, most likely in lysosomes (Fig. 1). The third series of experiments were aimed at investigating individual cell entry dynamics and intracellular distribution of ASO and doxorubicin. To this end, ASO were labeled with FITC (doxorubicin possesses intrinsic fluorescence) and living A2780/AD human multidrug-resistant ovarian carcinoma cells were incubated with liposomes containing ASO-FITC and doxorubicin. The fluorescence of ASO-FITC (green) and doxorubicin (red) were observed by a confocal microscope in living cells before treatment and at different time points after adding liposomes into the media. Fluorescence of FITC and doxorubicin was quenched by liposomes. Therefore, the presence of green and/or red fluorescence is a hallmark of the ASO-FITC or doxorubicin release from the liposomes, respectively. The superposition of green and red fluorescent images allows for investigating colocalization of ASO-FITC and doxorubicin, which creates a yellow color. Figure 3 shows the results of *in vitro* experiments which were carried out on living ovarian cancer cells at 37°C. No substantial fluorescence was detected before the application of conventional liposomes with encapsulated doxorubicin to the cells and after the first few minutes of the incubation of cells with liposomal doxorubicin. Several minutes after the injection of liposomal doxorubicin to the incubation medium, fluorescence was first seen near the plasma membrane and the adjacent cytoplasm. It seems that soon after the beginning of the incubation, part of the liposomes fuse with the plasma membrane or are destroyed near the plasma membrane, releasing ASO and doxorubicin from the liposomes near the plasma membrane. However, a few minutes later, the fluorescence of released doxorubicin became visible deep inside the cytoplasm, in a perinuclear region, and finally in the nucleus itself. Therefore, at the later stages, liposomes were internalized by endocytosis, doxorubicin and ASO were released from liposomes in the perinuclear

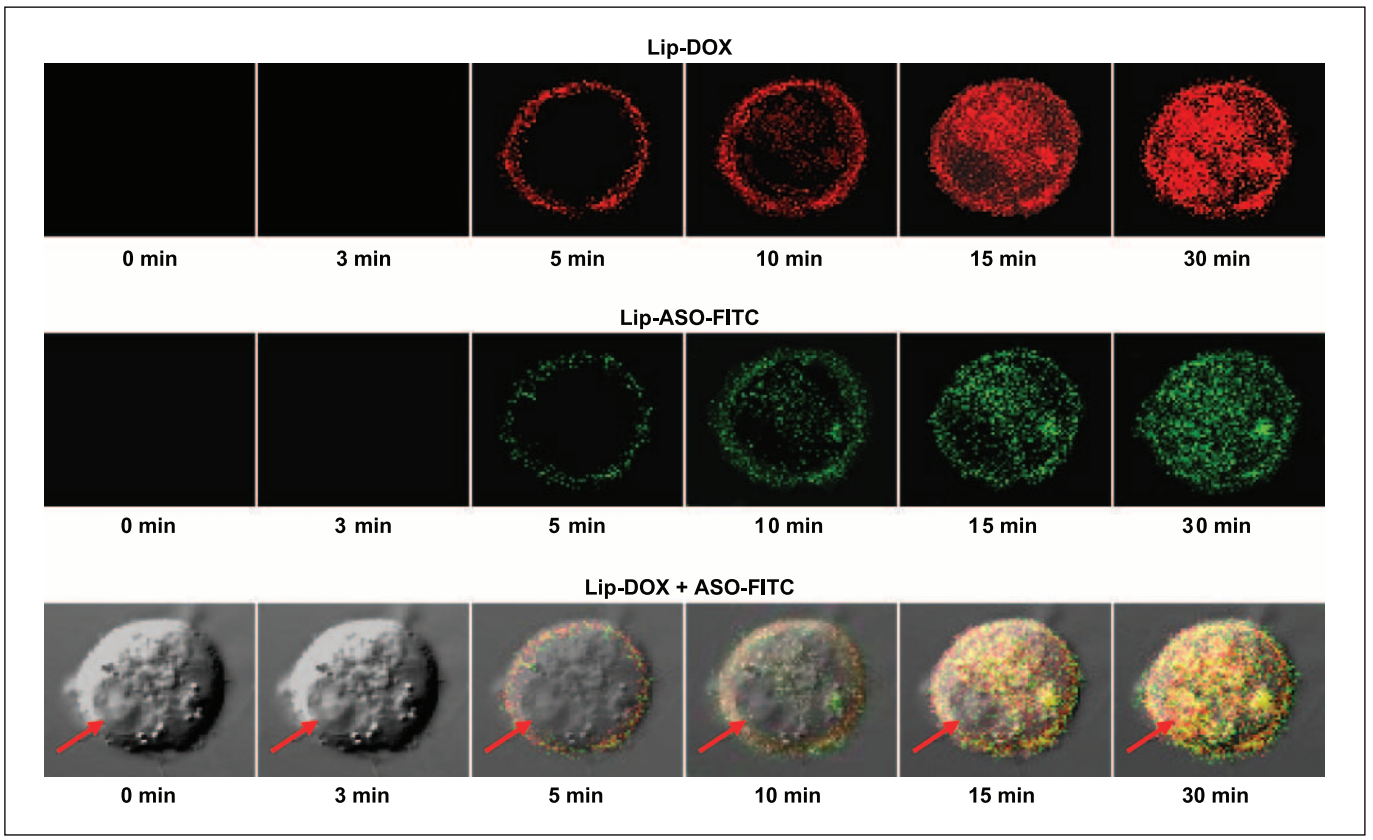

Fig. 3. Release of doxorubicin and ASO from PEGylated liposomes inside cancer cells. Confocal microscopy images of multidrug-resistant A2780/AD human ovarian cancer cells before and after incubation with PEGylated liposomes loaded with doxorubicin (*DOX, red*) and labeled with FITC antisense oligonucleotides (*ASO-FITC, green*). Bottom, the superposition of visible light images with fluorescence images of doxorubicin and ASO-FITC. Arrows, nucleus.

Downloaded from clincancerres.aacrjournals.org on September 21, 2019. © 2008 American Association for Cancer Research.

Table 1. Gene/protein expression in tumor tissue homogenates measured by quantitative RT-PCR and Western blotting

Series	Gene expression by RT-PCR					
	HIF1A	VHL	P53	HSP90	BAX	BCL2
Control	53.1 ± 2.4	68.9 ± 3.2	34.8 ± 1.6	13.2 ± 0.8	18.1 ± 0.4	35.1 ± 1.1
HIF1A ASO	50.6 ± 3.1	65.3 ± 4.0	36.1 ± 3.3	12.6 ± 2.4	19.4 ± 2.1	36.6 ± 3.8
Liposome	53.9 ± 3.1	69.2 ± 3.7	34.3 ± 1.3	12.9 ± 1.1	18.2 ± 0.5	34.9 ± 1.3
Liposomal HIF1A ASO	34.4 ± 1.7*	52.5 ± 2.7*	48.4 ± 2.1*	11.6 ± 1.8	17.8 ± 1.6	30.1 ± 1.4*
Free doxorubicin	89.7 ± 4.1*	104.1 ± 5.3*	62.5 ± 3.2*	76.4 ± 3.3*	58.0 ± 2.4*	71.0 ± 2.9*
Liposomal doxorubicin	81.3 ± 4.6*,†	86.0 ± 4.9*,†	78.4 ± 2.6*,†	58.6 ± 1.9*,†	65.9 ± 2.4*,†	54.2 ± 1.8*,†
Liposomal doxorubicin + HIF1A ASO	24.9 ± 1.7*,†,‡	70.2 ± 3.1†,‡	99.8 ± 4.1*,†,‡	28.2 ± 0.9*,†,‡	79.1 ± 3.0*,†,‡	36.7 ± 1.4†,‡

NOTE: The expression is presented as a percentage of the internal standard (β_2-microglobilin and β-actin for RT-PCR and Western blotting, respectively). The samples for the analysis were taken at the end of the experiments (day 6 after the treatment; mean ± SD).
*$P < 0.05$ when compared with control.
†$P < 0.05$ when compared with free doxorubicin.
‡$P < 0.05$ when compared with liposomal doxorubicin.

region and entered the nucleus, or loaded liposomes were internalized into the nucleus and released active ingredients (Fig. 3). Analysis of individual localization and colocalization of ASO and doxorubicin inside cells after their release from the liposomes showed that there were no substantial differences in the intracellular localization between ASO and doxorubicin. Both ingredients were distributed uniformly within the cytoplasm and nuclei (Fig. 3, composite images, bottom).

Intracellular liposomal delivery of ASOs targeted to HIF1A mRNA prevented the overexpression of HIF1A gene and protein induction by the anticancer drug. Analysis of HIF1A mRNA by RT-PCR and protein by the immunohistochemical staining of paraffin-embedded tumor tissues showed that treatment with free and liposomal doxorubicin led to the overexpression of mRNA and protein (Table 1; Fig. 4). The inclusion of ASO targeted to HIF1A mRNA into liposomal drug delivery systems prevents such overexpression and even resulted in a decrease in the expression of HIF1A when compared with the control level. It should be stressed that free ASO (nonencapsulated into liposomes) had a very limited ability to penetrate inside cells (27) and were not effective in the suppression of this protein in the tumor following systemic delivery (Table 1) and even in the *in vitro* setting (data not shown). Thus, delivery of ASO by liposomes enhanced their specific activity and prevented the overexpression of HIF1A protein in tumors induced by the anticancer drug.

The combination of the anticancer drug and ASO targeted to HIF1A mRNA in one liposomal delivery system amplified cell death signals induced by doxorubicin and inhibited cellular resistance against the anticancer drug. We analyzed cell death susceptibility and resistance in tumor cells by measuring the expression of genes and proteins involved in cell death signaling pathways (P53, BAX, CASP3, CASP9), and antiapoptotic defense and general nonspecific cellular resistance (HSP90, BCL2). In addition, we also analyzed the expression of vascular endothelial growth factor (VEGF), which is responsible for tumor angiogenesis, growth, and therefore, its resistance to chemotherapy. The data obtained show that free doxorubicin induced both pathways: tumor cell death induction and defense (Table 1). At the same time, it also dramatically stimulated VEGF expression. Delivery of doxorubicin by liposomes increased the induction of cell death signal by doxorubicin (up-regulation of P53, BAX, CASP9, CASP3) while moderately, but significantly, limiting VEGF overexpression in the tumor and cellular defensive mechanisms (down-regulation of BCL2 and HSP90). The inclusion of ASO targeted to HIF1A into the liposomal system containing doxorubicin further enhanced apoptotic signals and restricted cellular mechanisms responsible for tumor cell death defense. To characterize the equilibrium between proapoptotic cell death signal and antiapoptotic cellular defense, the BAX/BCL2 ratio was calculated. We found that after the combined action of doxorubicin and ASO targeted to HIF1A mRNA, this ratio was >4-fold higher when compared with the BAX/BCL2 ratio in the tumor of untreated animals and >2.5-fold and 1.7-fold higher when compared with this variable in the tumors of mice treated with free and liposomal doxorubicin alone, respectively (Table 1). It is important to note that the increase in cell death signal took place on the background of decreased nonspecific resistance that depends on the expression of heat shock protein HSP90. The increase in cell death signal led to the overexpression of caspase 9 and cleavage of procaspase 9 to form active caspase 9. The active caspase 9 (apoptosis initiator) triggered the cascade of caspase-apoptosis executors, including caspase 3. In addition, the combination of doxorubicin with ASO limited the VEGF expression by 2-fold when compared with free doxorubicin.

Liposomal ASO targeted to HIF1A mRNA enhanced the antitumor activity of doxorubicin. Analysis of cell death induction and antitumor activity of investigated preparations was done by several independent methods. First, tumor tissues were fixed, stained by H&E, and analyzed by light microscopy for signs of necrosis. Second, two methods of apoptosis analysis, terminal deoxynucleotidyl transferase mediated dUTP-fluorescein nick-end labeling and cell death ELISA, were applied to tumor tissues. Lastly, tumor size was measured daily for 7 consecutive days after treatment with the studied substances. Adverse side effects of the treatment were estimated by measuring apoptosis induction in heart and liver tissue samples. The data obtained show that the combination of doxorubicin with ASO targeted to HIF1A mRNA in one liposomal delivery system substantially

Downloaded from clincancerres.aacrjournals.org on September 21, 2019. © 2008 American Association for Cancer Research.

Table 1. Gene/protein expression in tumor tissue homogenates measured by quantitative RT-PCR and Western blotting (Cont'd)

Gene expression by RT-PCR		Protein expression by Western blotting		
BAX/BCL2	CASP3	Pro-CASP9	Active CASP9	VEGF
0.51 ± 0.02	39.9 ± 1.4	40.1 ± 1.7	0.56 ± 3.48	42.0 ± 1.4
0.52 ± 0.08	40.4 ± 3.6	41.2 ± 3.1	0.58 ± 4.09	43.7 ± 4.1
0.52 ± 0.02	38.9 ± 1.6	40.3 ± 1.9	0.5 ± 4.13	41.9 ± 1.2
0.60 ± 0.02*	48.8 ± 2.0*	50.2 ± 2.4*	12.1 ± 0.8*	35.4 ± 1.5*
0.82 ± 0.04*	60.3 ± 2.9*	74.5 ± 3.2*	28.2 ± 0.9*	136.1 ± 3.7*
1.22 ± 0.05* †	81.1 ± 3.7* †	110.3 ± 4.1* †	39.1 ± 1.0* †	97.2 ± 3.4* †
2.16 ± 0.09* † ‡	113 ± 4.6* † ‡	136.8 ± 4.3* † ‡	54.3 ± 1.9* † ‡	62.3 ± 2.6* † ‡

enhanced the ability of doxorubicin to induce necrosis in tumor tissues leading to an increase in the volume of tumor tissues with signs of necrosis (Fig. 5A). In addition to necrosis, ASO targeted to HIF1A mRNA also enhanced the induction of programmed cell death by doxorubicin. Both methods of apoptosis analysis (terminal deoxynucleotidyl transferase mediated dUTP-fluorescein nick-end labeling and cell death ELISA) gave comparable results, indicating the enhancement of proapoptotic activity of doxorubicin by HIF1A ASO (compare Fig. 5B and E). The apoptosis induction by the liposomal doxorubicin-ASO combination was >30-fold higher when compared with control, and 4-fold and >1.5-fold higher when compared with the treatment by free doxorubicin and liposomal doxorubicin, respectively. In contrast, liposomal ASO alone led to a rather moderate induction of apoptotic cell death. Finally, higher cell death induction of a multifunctional liposomal delivery system containing ASO targeted to HIF1A mRNA and doxorubicin resulted in considerably higher antitumor activity, leading to a significant decrease in tumor size even after only a single treatment (Fig. 5D). It should be stressed that doxorubicin and ASO targeted to HIF1A mRNA simultaneously delivered in one liposomal system (Fig. 5E and F, series 10) were significantly more effective in the induction of apoptosis and tumor shrinkage when compared with liposomal doxorubicin and liposomal ASO delivered separately in different liposomal formulations (Fig. 5E and F, series 9). At the same time, we did not find statistically significant differences in mice body weight between all studied experimental groups. Analysis of apoptosis in heart and liver showed that free doxorubicin induced cell death, not only in the tumor, but also in healthy organs (Fig. 5C-E, series 5). Simultaneous treatment of tumor-bearing animals with free doxorubicin and liposomal ASO resulted in similar adverse side effects of doxorubicin (Fig. 5C-E, series 6). Delivery of the same dose of doxorubicin as liposomal formulations substantially limited apoptosis induction in heart and liver and enhanced cell death in the tumor (Fig. 5C-E, series 7-10). The mixture of liposomal doxorubicin with liposomal ASO targeted to HIF1A mRNA was less effective and caused more pronounced adverse side effects in the heart and liver when compared with doxorubicin and ASO simultaneously delivered within the same liposome.

Discussion

Data obtained show that the proposed novel delivery system provided preferential accumulation of ASO and doxorubicin in the tumor of mice bearing xenografts of human multidrug-resistant ovarian carcinoma. Possible mechanisms of this phenomenon include the enhanced permeability and retention effect (28). The enhanced permeability and retention effect is the result of the increased permeability of the tumor vascular endothelium to circulating macromolecules combined with

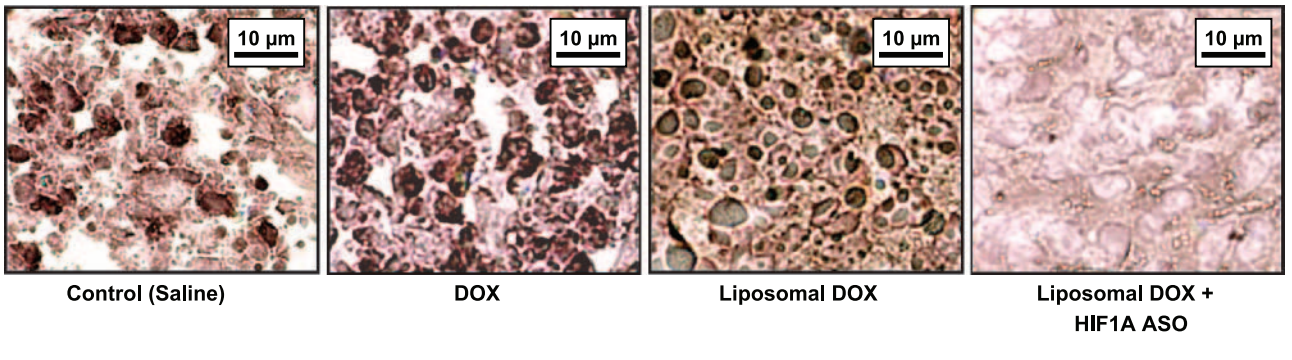

Fig. 4. HIF1A protein expression. Typical images of tumor tissue sections stained with antibody against HIF1A protein. Dark color indicates high protein concentration. Tumor tissue sections were obtained from mice bearing xenografts of multidrug-resistant A2780/AD human ovarian carcinoma and were treated with the indicated formulations. Samples for analysis were taken at the end of the experiments (day 6 after the treatment).

Downloaded from clincancerres.aacrjournals.org on September 21, 2019. © 2008 American Association for Cancer Research.

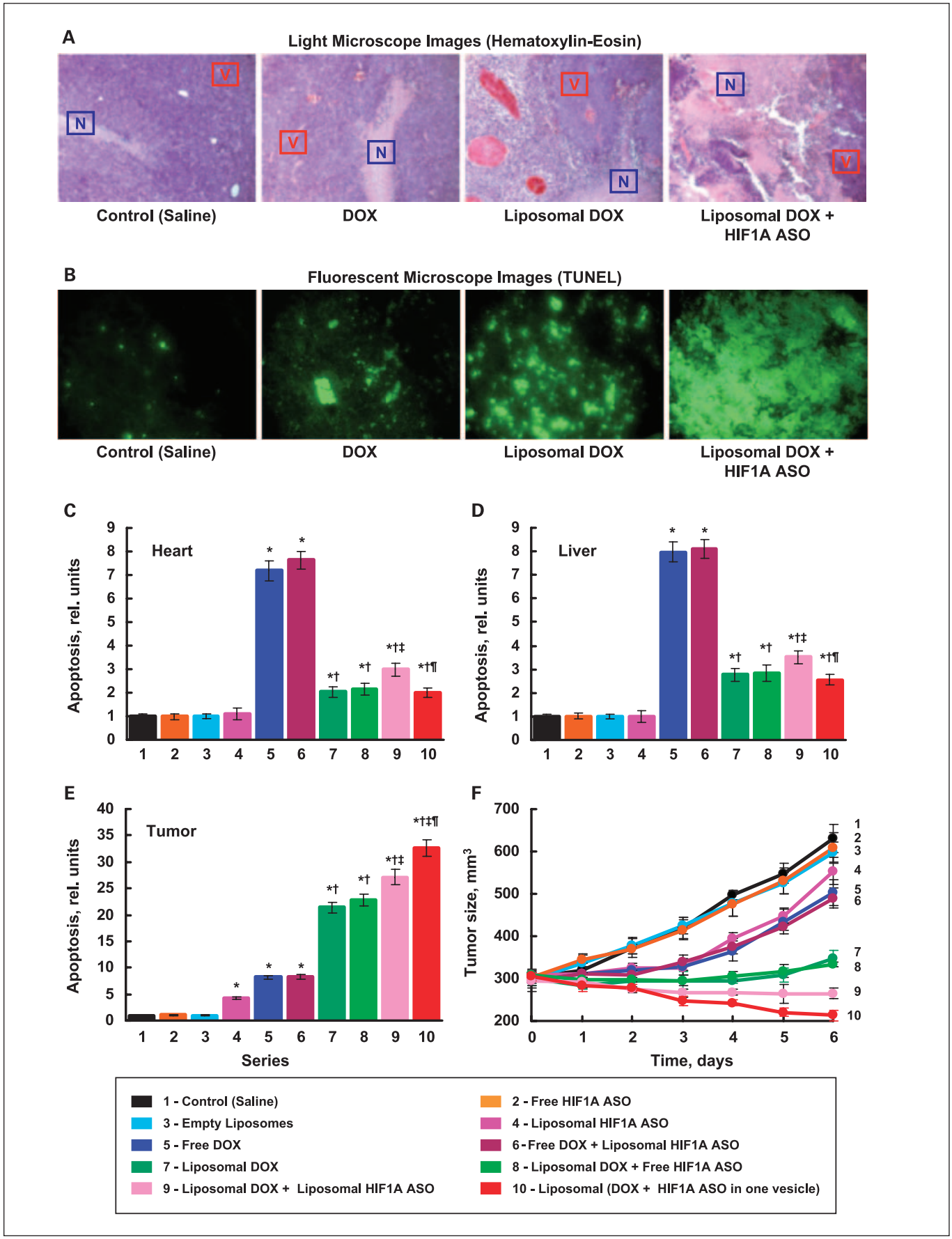

Downloaded from clincancerres.aacrjournals.org on September 21, 2019. © 2008 American Association for Cancer Research.

limited lymphatic drainage from the tumor interstitium. Because of the enhanced permeability and retention effect, low–molecular weight drugs coupled with high–molecular weight carriers are inefficiently removed by lymphatic drainage and therefore accumulate in the tumors. Moreover, we found that liposomes penetrated inside tumor cells in the tumor cytoplasm, releasing encapsulated doxorubicin and ASO in the cytoplasm, in the perinuclear area, and possibly in the nucleus. Analysis of the data obtained allows us to speculate that the main mechanism of cellular entry of the PEGylated liposomes is endocytosis. It seems that only a small fraction of liposomes released ASO and doxorubicin near the plasma membrane at the initial stage of the penetration, probably after fusion with the plasma membrane. After endocytosis, the liposomes were transferred through the cytoplasm inside endosomes and released their payload after the fusion of endosomes with lysosomes in the perinuclear region of the cells. Such mechanisms of cellular entry and trafficking inside membrane-limited organelles protects liposomes from premature destruction and limits the inactivation of encapsulated ASO and an anticancer drug by cytoplasmic enzymes. It allows deep cytoplasmic penetration of active doxorubicin and ASO and their release after the destruction of liposomes near nuclei providing for the highest possible activity in terms of suppressing the synthesis of targeted protein and cell death induction.

Previously, we and others reported that liposomal encapsulation of ASO or short interfering RNA improved their intracellular delivery and enhanced the ability of ASO and short interfering RNA in suppression of the expression of targeted proteins (27). Data obtained in the present study *in vivo* on mice bearing xenografts of human multidrug-resistant ovarian carcinoma support our previous *in vitro* findings. The data also show that the delivery of ASO by PEGylated liposomes prevented the overexpression of targeted HIF1A protein activated by treatment with free and liposomal doxorubicin. This can potentially trigger two types of cellular response (8). First, it might decrease the cell death signal induced by tumor hypoxia and possibly by an anticancer drug. Second, it can inhibit the resistance of tumor cells both to internal tumor hypoxia and the external action of an anticancer drug. Based on our previous results, we hypothesized that the negative influence on cell death signal would be minimal and the suppression of cellular resistance will prevail. The current experimental data fully support this hypothesis. Analysis of mRNA and proteins involved in apoptosis induction and suppression by anticancer drugs and other external stimuli showed that the combination of doxorubicin with HIF1A ASO in one liposomal delivery system led to the simultaneous induction of cell death by doxorubicin and suppression of cellular resistance and angiogenesis by ASO. Previously, we found that the same combination of active ingredients did not change the intrinsic multidrug resistance of A2780/AD human ovarian carcinoma cells depending on P-glycoprotein expression and substantially limited the overexpression of multidrug-resistant–associated protein 1, which determines another component of multidrug resistance in these cells (19). Taken together, these data indicate that the combination of doxorubicin with ASO targeted to HIF1A mRNA in one liposomal delivery system enhances the ability of doxorubicin to induce cell death by activating major signaling pathways of apoptosis and necrosis and inhibiting all aspects of cellular resistance to chemotherapy including multidrug resistance, nonspecific resistance, and antiapoptotic cellular defense. As a result, the induction of both types of cell death, apoptosis and necrosis, by the liposomal HIF1A ASO-doxorubicin combination in tumor tissues was significantly higher when compared with free and liposomal doxorubicin. Therefore, we were able to verify our hypothesis and show that the suppression of HIF1A protein substantially enhanced the antitumor activity of the anticancer drug.

Analysis of apoptosis induction in the heart and liver revealed severe adverse effects of free doxorubicin on healthy tissues. Delivery of doxorubicin as liposomal formulations substantially limited these effects, possibly by a preferential accumulation of liposomes in tumor by the enhanced permeability and retention effect. It should be stressed that liposomal doxorubicin and liposomal ASO administered at the same time, but in different formulations, showed lower antitumor activity and higher adverse side effects on healthy tissues when compared with liposomes containing both doxorubicin and ASO in one vesicle. The following explanation of such an observation could be proposed. To reach the same concentrations of active ingredients inside tumor cells (when compared with simultaneous delivery of doxorubicin and ASO in the same liposomal vesicle), twice the number of liposomes should penetrate into the cells when doxorubicin and ASO are delivered in separate liposomes. However, the capacity of endocytosis in terms of the internalization of exogenous vesicles is limited. Consequently, one can hypothesize that such a limitation in endocytosis could explain the decrease in the antitumor activity and contribute to pronounced adverse side effects of chemotherapy if doxorubicin and ASO were delivered in separate liposomal vesicles. Although detailed mechanisms of such effects require more thorough investigations, the present study clearly showed that doxorubicin and HIF1A ASO, delivered together in the same liposomal vesicle, increased the efficacy of cancer chemotherapy to a level that cannot be achieved by separate treatment with individual components.

In summary, the proposed novel approach to cancer chemotherapy is based on the simultaneous induction of cell death by the anticancer agents and the suppression of cellular resistance and angiogenesis by the inhibition of HIF1A-dependent cellular signaling. In addition, this approach uses tumor hypoxia as an additional therapeutic factor by the suppression of antihypoxic defensive mechanisms in tumor cells. Simultaneous induction of cell death and suppression of HIF1A protein is achieved by combining an anticancer drug and ASO targeted to HIF1A mRNA into one liposomal delivery

Fig. 5. Cell death and tumor growth. Mice bearing xenografts of multidrug-resistant A2780/AD human ovarian carcinoma were treated with the indicated formulations. Samples for analysis were taken at the end of the experiments (day 6 after the single treatment). *A,* light microscopy images of tumor tissue sections stained with H&E. Necrotic (*N*) and viable (*V*) regions of tumor tissue. *B,* fluorescent microscopy images of terminal deoxynucleotidyl transferase mediated dUTP-fluorescein nick-end labeling (TUNEL)–labeled tumor sections. *C,* apoptosis induction in heart tissues. *D,* apoptosis induction in liver tissues. *E,* apoptosis induction in tumor tissues. The enrichment of histone-associated DNA fragments (mononucleosomes and oligonucleosomes) in control (untreated tumors) was set to unit 1, and the degree of apoptosis was expressed in relative units. *F,* tumor size. Points, mean; bars, SD. *, $P < 0.05$ when compared with control (*saline, series 1*); †, $P < 0.05$ when compared with free doxorubicin (*series 5*); ‡, $P < 0.05$ when compared with liposomal doxorubicin (*series 7*); ¶, $P < 0.05$ when compared with liposomal doxorubicin + liposomal HIF1A ASO (*series 9*).

Downloaded from clincancerres.aacrjournals.org on September 21, 2019. © 2008 American Association for Cancer Research.

system. Such a nanoscale-based nonviral delivery system provides an effective delivery of active ingredients into tumor cells and enhances both the cell death–inducing activity of the anticancer drug and the suppression of targeted protein by ASO. The proposed approach will form the foundation for a novel type of cancer therapy based on the simultaneous delivery of a suppressor of HIF1A and an anticancer drug. It is expected that such combination therapy will prevent the development of resistance in cancer cells, and thus, will increase the efficacy of chemotherapy to an extent that cannot be achieved by individual components applied separately.

References

1. Minko T, Kopeckova P, Kopecek J. Chronic exposure to HPMA copolymer-bound adriamycin does not induce multidrug resistance in a human ovarian carcinoma cell line. J Control Release 1999;59:133–48.
2. Fennelly D. Dose intensity in advanced ovarian cancer: have we answered the question? Clin Cancer Res 1995;1:575–82.
3. Searcey M, Patterson LH. Resistance in cancer: a target for drug discovery. Curr Med Chem Anticancer Agents 2004;4:457–60.
4. Brown JM. Tumor microenvironment and the response to anticancer therapy. Cancer Biol Ther 2002;1:453–8.
5. Harris AL. Hypoxia—a key regulatory factor in tumour growth. Nat Rev Cancer 2002;2:38–47.
6. Shannon AM, Bouchier-Hayes DJ, Condron CM, Toomey D. Tumour hypoxia, chemotherapeutic resistance and hypoxia-related therapies. Cancer Treat Rev 2003;29:297–307.
7. Wouters BG, Koritzinsky M, Chiu RK, Theys J, Buijsen J, Lambin P. Modulation of cell death in the tumor microenvironment. Semin Radiat Oncol 2003;13:31–41.
8. Wang Y, Pakunlu RI, Tsao W, Pozharov V, Minko T. Bimodal effect of hypoxia in cancer: the role of hypoxia inducible factor in apoptosis. Mol Pharmacol 2004;1:156–65.
9. Tsuruo T, Naito M, Tomida A, et al. Molecular targeting therapy of cancer: drug resistance, apoptosis and survival signal. Cancer Sci 2003;94:15–21.
10. Brunelle JK, Chandel NS. Oxygen deprivation induced cell death: an update. Apoptosis 2002;7:475–82.
11. Kietzmann T, Knabe W, Schmidt-Kastner R. Hypoxia and hypoxia-inducible factor modulated gene expression in brain: involvement in neuroprotection and cell death. Eur Arch Psychiatry Clin Neurosci 2001;251:170–8.
12. Knowles HJ, Harris AL. Hypoxia and oxidative stress in breast cancer. Hypoxia and tumourigenesis. Breast Cancer Res 2001;3:318–22.
13. Pluquet O, Hainaut P. Genotoxic and non-genotoxic pathways of p53 induction. Cancer Lett 2001;174:1–15.
14. Escuin D, Simons JW, Giannakakou P. Exploitation of the HIF axis for cancer therapy. Cancer Biol Ther 2004;3:608–11.
15. Yu JL, Coomber BL, Kerbel RS. A paradigm for therapy-induced microenvironmental changes in solid tumors leading to drug resistance. Differentiation 2002;70:599–609.
16. Ryan HE, Poloni M, McNulty W, et al. Hypoxia-inducible factor-1α is a positive factor in solid tumor growth. Cancer Res 2000;60:4010–5.
17. Brune B, von Knethen A, Sandau KB. Transcription factors p53 and HIF-1α as targets of nitric oxide. Cell Signal 2001;13:525–33.
18. Livingston DM, Shivdasani R. Toward mechanism-based cancer care. JAMA 2001;285:588–93.
19. Wang Y, Minko T. A novel cancer therapy: combined liposomal hypoxia inducible factor 1α antisense oligonucleotides and an anticancer drug. Biochem Pharmacol 2004;68:2031–42.
20. Pakunlu RI, Wang Y, Tsao W, Pozharov V, Cook TJ, Minko T. Enhancement of the efficacy of chemotherapy for lung cancer by simultaneous suppression of multidrug resistance and antiapoptotic cellular defense: novel multicomponent delivery system. Cancer Res 2004;64:6214–24.
21. Dharap SS, Wang Y, Chandna P, et al. Tumor-specific targeting of an anticancer drug delivery system by LHRH peptide. Proc Natl Acad Sci U S A 2005;102:12962–7.
22. Dharap SS, Chandna P, Wang Y, et al. Molecular targeting of BCL2 and BCLXL proteins by synthetic BH3 peptide enhances the efficacy of chemotherapy. J Pharmacol Exp Ther 2006;316:992–8.
23. Minko T, Kopeckova P, Kopecek J. Efficacy of the chemotherapeutic action of HPMA copolymer-bound doxorubicin in a solid tumor model of ovarian carcinoma. Int J Cancer 2000;86:108–17.
24. Pakunlu RI, Wang Y, Saad M, Khandare JJ, Starovoytov V, Minko T. *In vitro* and *in vivo* intracellular liposomal delivery of antisense oligonucleotides and anticancer drug. J Control Release 2006;114:153–62.
25. Leclere P, Hennebicq E, Calderone A, et al. Supramolecular organization in block copolymers containing a conjugated segment: a joint AFM/molecular modeling study. Prog Polym Sci 2003;28:55–81.
26. Vetcher A, Gearheart R, Morozov V. Correlation of morphology of electrospun fibers with rheology of linear polyacrylamide solution. Polymer J 2007;39:1–4.
27. Betigeri S, Pakunlu RI, Wang Y, Khandare JJ, Minko T. JNK1 as a molecular target to limit cellular mortality under hypoxia. Mol Pharmacol 2006;3:424–30.
28. Maeda H. The enhanced permeability and retention (EPR) effect in tumor vasculature: the key role of tumor-selective macromolecular drug targeting. Adv Enzyme Regul 2001;41:189–207.

Downloaded from clincancerres.aacrjournals.org on September 21, 2019. © 2008 American Association for Cancer Research.

AACR American Association for Cancer Research

Clinical Cancer Research

Nonviral Nanoscale-Based Delivery of Antisense Oligonucleotides Targeted to Hypoxia-Inducible Factor 1 α Enhances the Efficacy of Chemotherapy in Drug-Resistant Tumor

Yang Wang, Maha Saad, Refika I. Pakunlu, et al.

Clin Cancer Res 2008;14:3607-3616.

Updated version Access the most recent version of this article at:
http://clincancerres.aacrjournals.org/content/14/11/3607

Cited articles This article cites 28 articles, 4 of which you can access for free at:
http://clincancerres.aacrjournals.org/content/14/11/3607.full#ref-list-1

E-mail alerts Sign up to receive free email-alerts related to this article or journal.

Reprints and Subscriptions To order reprints of this article or to subscribe to the journal, contact the AACR Publications Department at pubs@aacr.org.

Permissions To request permission to re-use all or part of this article, use this link
http://clincancerres.aacrjournals.org/content/14/11/3607.
Click on "Request Permissions" which will take you to the Copyright Clearance Center's (CCC)
Rightslink site.

Downloaded from clincancerres.aacrjournals.org on September 21, 2019. © 2008 American Association for Cancer Research.